Rashba semiconductor as spin Hall material: Experimental demonstration of spin pumping in wurtzite *n*-GaN:Si

R. Adhikari,[1,2,*] M. Matzer,[1,2] A. Tarazaga Martín-Luengo,[1,2] M. C. Scharber,[2,3] and A. Bonanni[1,2,†]

[1]*Institut für Halbleiter-und-Festkörperphysik, Johannes Kepler University, Altenbergerstrasse 69, A-4040 Linz, Austria*

[2]*Linz Institute of Technology (LIT), Johannes Kepler University, Altenbergerstrasse 69, A-4040 Linz, Austria*

[3]*Linz Institute for Organic Solar Cells, Johannes Kepler University, Altenbergerstrasse 69, A-4040 Linz, Austria*

(Received 1 April 2016; revised manuscript received 16 August 2016; published 31 August 2016)

Pure spin currents in semiconductors are essential for implementation in the next generation of spintronic elements. Heterostructures of III-nitride semiconductors are currently employed as central building blocks for lighting and high-power devices. Moreover, the long relaxation times and the spin-orbit coupling (SOC) in these materials indicate them as privileged hosts for spin currents and related phenomena. Spin pumping is an efficient mechanism for the inception of spin current and its conversion into charge current in nonmagnetic metals and semiconductors with Rashba SOC. We report on the generation at room temperature (RT) of pure spin current in nonmagnetic degenerate *n*-GaN:Si from a magnetic permalloy layer driven to ferromagnetic resonance (FMR) conditions. The FMR signal and the generated Hall voltages due to spin Hall effect, inverse spin Hall effect (ISHE), and spurious mechanisms are detected simultaneously. No spin-pumping-induced voltage could be measured below RT, despite the persistence of FMR signal. After eliminating the spurious (not due to ISHE) components contributing to the generated voltage, we find for *n*-GaN:Si a spin Hall angle $\theta_{SH} = 3.03\times10^{-3}$, exceeding by one order of magnitude those reported for other semiconductors, pointing at III-nitrides as particularly efficient spin current generators.

DOI: 10.1103/PhysRevB.94.085205

I. INTRODUCTION

In the emerging field of spin-orbitronics [1–4], spin-orbit coupling (SOC) is employed in both magnetic and nonmagnetic materials to generate, exploit, and detect spin currents. Spin currents hold the key for the realization and implementation of the next generation of spin-based nanoelectronic devices with properties such as nonvolatility, low power consumption, and dissipation. While in magnetic materials the SOC is employed to create new classes of topological objects such as magnetic skyrmions or Dzyalonshinskii-Moriya domain walls [1,5], spin-orbitronics in nonmagnetic materials mostly addresses the spin-to-charge conversion through the spin Hall effect (SHE) [6] and the Rashba-Edelstein effect [7,8]. The concept of SHE is borrowed from the anomalous Hall effect (AHE) where, due to the relativistic SOC, asymmetric deflection of charge carriers takes place depending on their spin orientations [9]. While AHE is studied in magnetic systems, SHE is mostly observed in nonmagnetic ones. Based on the concept of spin-dependent Mott scattering [10], the SHE was predicted nearly four decades ago by D'yakonov and Perel' [11] and was proposed to be the effective process for producing pure spin currents in solid state systems. However, it was not until the theoretical work of Hirsch *et al.* [12] and Zhang *et al.* [13] that the extrinsic SHE received renewed attention. The possibility of an intrinsic mechanism was proposed by various theoretical groups [14–16]. The intrinsic SHE depends only on the electronic band structure of the material. This effect arises from the nonequilibrium dynamics of the Bloch electrons as they undergo spin precession due to an induced *k*-dependent effective magnetic field, such as the Rashba field. The extrinsic SHE, on the other hand, is the mechanism in which the spins acquire transverse velocity due to SOC during scattering of electrons [6,9,17]. The extrinsic SHE is classified according to two different underlying mechanisms, viz., the skew scattering and the side jump mechanism. Skew scattering is the asymmetric scattering of spin, within the scattering plane, due to an effective magnetic field gradient that arises as an effect of the SOC. The scattering plane defines the spin polarization direction of the resulting spin current. The side jump mechanism is the velocity integrated over time of deflection of electrons in opposite directions by the electric fields experienced when approaching or withdrawing an impurity. This phenomenon results in an effective transverse displacement of the electrons upon multiple scattering events. At low carrier mobilities $\sim(10^{-2}$ to $10^{2})$ cm^2 V^{-1} s^{-1}, the intrinsic and extrinsic side jump mechanisms contribute mostly to the SHE, while for carrier mobilities greater than 10^2 cm^2 V^{-1} s^{-1}, extrinsic skew scattering is the dominant process [6,17]. Moreover, for mobilities exceeding 10^3 cm^2 V^{-1} s^{-1}, spin Coulomb drag becomes the dominant mechanism [17] and compels the spin Hall conductivity towards a saturation value. The lack of direct electrical signals proved to be a major challenge in the observation of this effect, so that the initial experimental efforts were mostly accomplished using optical means [18–20].

In a series of seminal publications, Tserkovnyak, Brataas, and Bauer [21–23] suggested a method for obtaining pure spin current in nonmagnetic (NM) metals and semiconductors with non-negligible SOC. They proposed a spin battery [23] based on adiabatic pumping of spins from a ferromagnetic metal or insulator (FM) grown in a FM/NM bilayer configuration when the system is driven to resonance under microwave irradiation. Such a battery leads to the dynamic generation of pure spin current in a NM with nontrifling SOC via ferromagnetic resonance (FMR) of the FM [24]. The magnetization dynamics

*rajdeep.adhikari@jku.at

†alberta.bonanni@jku.at

of ferromagnets is well described by the phenomenological Landau-Lifshitz-Gilbert (LLG) equation [25]:

$$\frac{d\vec{M}(t)}{dt} = -\gamma \vec{M}(t) \times \vec{H}_{\text{eff}} + \frac{\alpha}{M_s}\vec{M}(t) \times \frac{d\vec{M}(t)}{dt}, \quad (1)$$

where $\vec{M}(t)/M_s$ is the unit vector of magnetization, γ the gyromagnetic ratio, and $\vec{H}_{\text{eff}}$ the effective magnetic field expressed as $\vec{H}_{\text{eff}} = \vec{H} + \vec{H}_M(t) + \vec{h}(t)$, with $\vec{H}$ the external magnetic field, $\vec{H}_M(t)$ the dynamic demagnetizing field, and $\vec{h}_{MW}(t)$ the ac field due to microwave radiation. The magnetization $\vec{M}(t)$ is expressed as a sum of the static and dynamic components, i.e., $\vec{M}(t) = \vec{M} + \vec{m}(t)$, and the dimensionless coefficient α is the Gilbert damping parameter. The first term on the right-hand side of Eq. (1) is the precession term, while the second term represents a damping component that impels the precession of magnetization $\vec{M}(t)$ to spiral down to a static magnetization axis due to the Gilbert damping parameter α. In a FM/NM hybrid bilayer, α is enhanced due to the transfer of spin angular momentum from the FM to the NM through a dynamical process of adiabatic spin pumping [22,24,26,27]. The spins pumped in the NM are scattered by the effective spin-orbit field; i.e., the Rashba field and a spin accumulation are achieved in the NM, leading to a spin current in the NM through SHE. An enhanced α in a FM/NM bilayer is a signature of spin pumping and a fingerprint of the generation of pure spin current in the NM. The spin current is converted into charge current, through a reciprocal process called the inverse spin Hall effect (ISHE) via the relation $\vec{J}_c = \theta_{SH}\vec{J}_s \times \vec{\sigma}$, where θ_{SH} is the spin Hall angle representing the efficiency of spin-to-charge conversion of a material. The charge current in the NM with SOC induces an electromotive force (emf), whose direction is perpendicular to the spin current $\vec{J}_s$ and to the spin polarization vector $\vec{\sigma}$. Spin pumping is an efficient mechanism to convert spin current into charge current without any applied bias. Over the last few years several experimental works have been published demonstrating spin pumping in heavy metals such as Pt [26,28–31], Ta [32,33], Pd [31,34], and Au [35], in semiconductors such as GaAs [36,37], Si [34,38], Ge [39], and ZnO [40,41], and recently also in 3-dimensional topological insulators [42] and ferroelectric Rashba semiconductors [43]. Apart from ferromagnetic spin pumping from a metallic FM such as permalloy (Py), it was also shown that spin currents can be realized in bilayers such as Pt/YIG [44–46] based on ferromagnetic insulators. Recent reports also point to spin pumping from paramagnets [47] and antiferromagnets [48,49]. The successful generation and control of spin current in semiconductors using the mechanism of spin pumping would open wide perspectives for the integration of spin functionalities in state-of-the-art electronic and optoelectronic devices based on semiconductors such as Si, Ge, III-nitrides, and III-arsenides.

Among the conventional III-V semiconductors, GaN and its alloys AlGaN and InGaN have emerged as strategic materials for optoelectronic and electronic applications, primarily due to their tunable wide band gap and structure-induced polarization. Furthermore, transition-metal-doped III-nitrides have been studied extensively in the past decade as workbench magnetic semiconductors [50,51]. Another fundamental aspect, namely the presence of Rashba spin-orbit coupling (RSOC) [52,53], was recently demonstrated in degenerate wurtzite (wz) *n*-GaN:Si [54]. Using magnetotransport measurements we have previously shown that the Rashba parameter, α_R, linear in k and accounting for the spin splitting of the conduction band in wz-GaN, has a value measured for *n*-GaN:Si to be (4.5 ± 1.0) meVÅ, i.e., the same magnitude found for a 2-dimensional electron gas (2DEG) formed at the AlGaN/GaN interface [54]. There, we demonstrated that in polar wz-GaN, the inversion asymmetry associated with the wurtzite crystal structure dominates over the interfacial electric field in the conduction band of GaN. The RSOC in degenerate *n*-GaN:Si makes this material a spin Hall system for prospective spin-orbitronic applications based on III-nitride semiconductors. Here, we report on the generation of pure spin currents in *n*-GaN:Si using an adiabatic spin pumping technique and we estimate the spin Hall angle for *n*-GaN:Si. The evaluation of the spin-to-charge conversion efficiency in *n*-GaN:Si opens up the possibility to design and implement high-performance spin-based III-nitride nanoelectronic and optoelectronic devices.

II. SAMPLES AND EXPERIMENTAL DETAILS

The experiments we report here have been performed on degenerately doped *n*-GaN:Si films with electron concentration $\sim(1.2\times10^{19})$ cm^{-3} and carrier mobility $\mu \sim 180$ cm^2 V^{-1} s^{-1}. The Si-doped GaN layers have been grown in an AIXTRON 200RF horizontal tube metal organic vapor phase epitaxy (MOVPE) reactor. The layers are deposited on a *c*-Al_2O_3 substrate using TMGa, NH_3, and SiH_4 as precursors for Ga, N, and Si, respectively, with H_2 as carrier gas. Following the nitridation of the sapphire substrate, a low-temperature nucleation layer (NL) is deposited at 540 °C and then annealed at 1040 °C. Then a 1.0-μm-thick GaN buffer layer is grown also at 1040 °C and finally the GaN:Si films of thickness between 150 nm and 1.9 μm are grown onto the GaN buffer layer at 1000 °C. All steps of the epitaxial process are monitored with *in situ* spectroscopic and kinetic ellipsometry. The systematic structural characterization of the layers with atomic force microscopy (AFM), high-resolution x-ray diffraction (HRXRD), and high-resolution transmission electron microscopy (HRTEM) confirms the high crystallinity of the samples and a rms roughness ≈1 nm.

A 10 nm permalloy (Py = $Ni_{80}Fe_{20}$) film [55] is used as the FM layer and source of spins. The Py film is passivated with a 6 nm AlO_x film which protects the FM from oxidation in order to avoid the detrimental effects of oxidized Py on the spin pumping efficiency [56]. The Al and the Py layers are deposited using an e-beam metallization chamber with 99.999% $Ni_{80}Fe_{20}$ and Al pellets as the target material. After air exposure, the Al layer is oxidized to form an AlO_x capping layer on Py. The chemical stoichiometry of the Py is analyzed by x-ray photoelectron spectroscopy (XPS) and details can be found in the Supplemental Material [57]. The Py/*n*-GaN:Si bilayer is driven to resonance conditions under an X-band microwave excitation of (9.40 ± 0.10) GHz with an external magnetic field. The permalloy—being a soft FM—has a small magnetocrystalline anisotropy, so that $\vec{M}(t)$ in Py is aligned along the film plane when an in-plane magnetic field $\vec{H}$ is applied.

The room temperature (RT) ferromagnetic resonance (FMR) studies have been carried out in a Bruker Elexsys E580 electron paramagnetic resonance spectrometer while the low-temperature measurements are performed with a Bruker EMX spectrometer equipped with a continuous flow He cryostat. In both the systems, the samples are mounted on a quartz rod and placed near the center of a TE_{011} cavity. An X-band microwave cavity is employed and measurements are performed at a frequency of (9.40 ± 0.10) GHz. An external magnetic field is swept from 0 to 1.3 T and an ac modulation field of 0.05 mT at 100 kHz is superimposed to obtain the FMR spectrum of the microwave absorption. The samples are cut in (10×4) mm^2 rectangles with the oxide-passivated Py layer being deposited over an area of (4×3) mm^2 while the Ti/Au/Al/Ti/Au Ohmic contacts are fabricated by means of e-beam evaporation at the long edges of the sample. The quartz sample holder for the FMR measurements is provided with two high-conducting copper wires and connected to a Keithley 2700 DMM for measuring the generated dc voltage, while the I-V characteristics for the FM/NM interfaces are recorded with Keithley SCS 4200 High Power SMUs. The voltage acquisition is synchronized with the external magnetic field sweep and with the microwave absorption spectrum. The dc voltage due to inverse spin Hall, thermal, and galvanomagnetic effects is measured and the value of the component due to inverse spin Hall effect is employed to calculate the spin Hall angle in n-GaN:Si. Control experiments are also performed on contacted n-GaN:Si without Py, on Py/c-Al_2O_3, Py/u-GaN, on bare c-Al_2O_3 substrates, and on the wired sample holder solely. Also, before the temperature-dependent FMR measurements with the Bruker EMX spectrometer, the RT measurements have been repeated and compared with the RT FMR and spin pumping data measured on the Elexsys 500 spectrometer. The θ_{SH} for each sample using the spin pumping data measured on the two different spectrometers are estimated and found to be consistent. This step is essential to ensure that there are no artifacts in the recorded data due to a change of the spectrometer conditions. No measurable voltage or FMR absorption has been detected from these test samples and control experiments, ruling out experimental artifacts affecting the observed results. A summary of the characteristics of the samples used for this study is reported in Table I.

TABLE I. Samples A–H: structure, NM layer thickness (d_N), carrier concentration (n_c) in NM layer, and Py/NM interface at room temperature.

Sample	Structure	d_N (μm)	n_c in NM layer (cm^{-3})	Py/NM interface
A	Py/c-Al_2O_3			Insulating
B	Py/u-GaN	1.00	3.0×10^{16}	Schottky
C	Py/n-GaN:Si	1.90	1.2×10^{19}	Ohmic
D	Py/n-GaN:Si	1.70	1.2×10^{19}	Ohmic
E	Py/n-GaN:Si	1.30	1.2×10^{19}	Ohmic
F	Py/n-GaN:Si	1.00	1.2×10^{19}	Ohmic
G	Py/n-GaN:Si	0.75	1.2×10^{19}	Ohmic
H	Py/n-GaN:Si	0.15	1.2×10^{19}	Ohmic

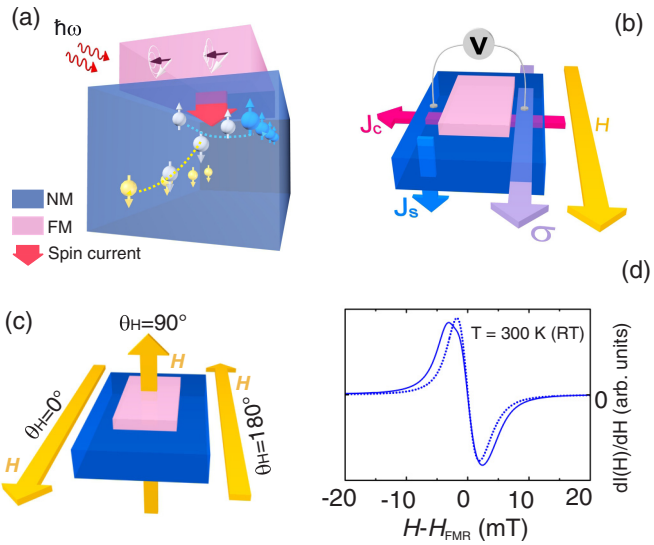

FIG. 1. (a) Spin pumping mechanism; (b) sample structure and schematic illustration of the physical quantities describing the spin pumping and spin current generation and detection through the Ohmic contacts on n-GaN:Si; (c) orientations of the applied magnetic field with respect to the sample surface; and (d) $\vec{H}$ dependence of the FMR signals $dI(H)/dH$ measured at $T = 300$ K for Py/c-Al_2O_3 and Py/n-GaN:Si bilayer at $\theta_H = 0°$.

III. DETECTION OF SPIN HALL EFFECT IN n-GaN:Si

Schematic representations of the spin pumping mechanism and of the geometry employed for the detection of the generated spin current in the NM are shown in Figs. 1(a) and 1(b), respectively. The sketches depict the magnetization precession in the FM for an applied magnetic field $\vec{H}$ at resonance condition under microwave excitation, leading to the pumping of spin angular momentum and subsequent generation of spin and charge currents in the NM through the SHE and ISHE. Measurements are carried out with the magnetic field applied in the in-plane and out-of-plane configuration, respectively.

Spin pumping is quenched for a perpendicular magnetic field and the angle-dependent measurement of the emf is essential to rule out secondary effects or experimental artifacts. The direction of the applied magnetic field with respect to the sample plane is indicated in Fig. 1(c), while the first derivative of the FMR signal for Py/c-Al_2O_3 (sample A) and Py/n-GaN:Si/c-Al_2O_3 (sample C) is provided in Fig. 1(d). The dotted and solid lines represent the FMR line shapes for the Py/c-Al_2O_3 and for the Py/n-GaN:Si bilayer, respectively. The broadening of the FMR signal for the Py/GaN:Si bilayer with respect to the reference Py/c-Al_2O_3 is the evidence of adiabatic spin pumping from the ferromagnetic Py into the Rashba semiconductor n-GaN:Si under resonance conditions [24,26,39]. The FMR signal and the electric potential difference between the electrodes attached to the n-GaN:Si layer are measured to detect the ISHE.

An enhancement of α characterized by a broadening of the FMR linewidth at resonance for a FM/NM bilayer with respect to the one for the bare FM layer is a signature of spin pumping. However, also the FM/NM interface properties

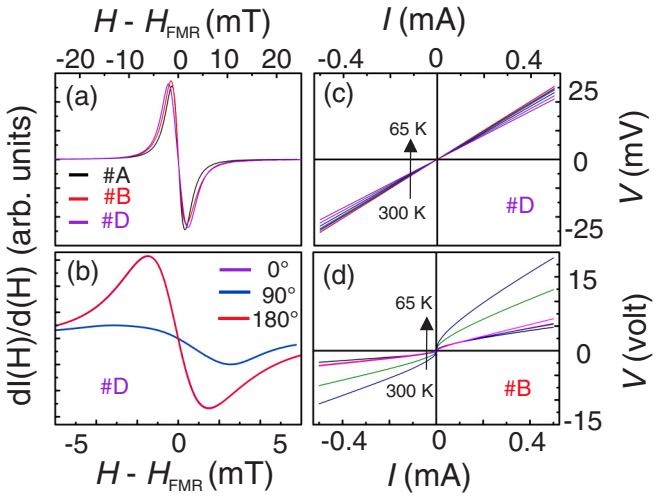

FIG. 2. (a) FMR spectra for samples A, B, and D measured at RT; (b) $\vec{H}$ dependence of the FMR signals $dI(H)/dH$ measured at $T = 300$ K for sample D at $\theta_H = 0°$, $\theta_H = 180°$, and $\theta_H = 90°$; temperature-dependent I-V characteristics for (c) Py/n-GaN:Si (sample D) and (d) Py/u-GaN (sample B) interfaces.

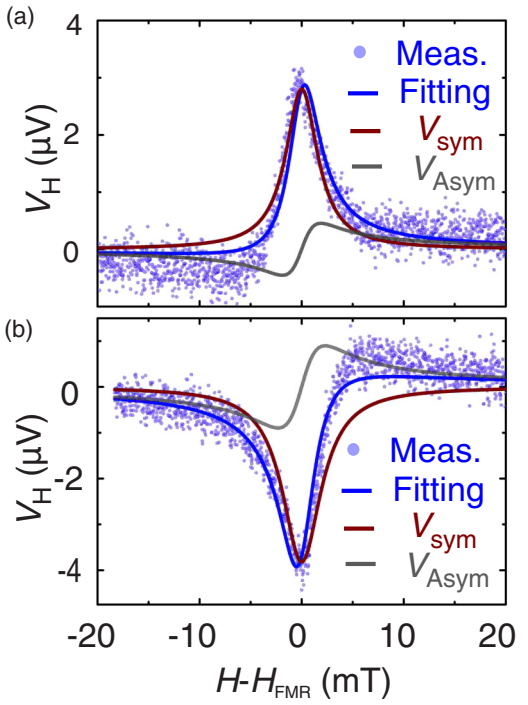

FIG. 3. Voltage across the electrodes on n:GaN:Si layer (sample C) for in-plane magnetic field orientations at (a) $\theta_H = 0°$ and (b) $\theta_H = 180°$ for $P_{MW} = 200$ mW. Dots: experimental data; solid lines: fitting according to Eq. (2).

and the electrical conductivity of the FM and NM layers determine the efficiency of transfer of the spin angular momentum from the FM to the NM. The FMR spectra for an in-plane magnetic field under identical resonance conditions for Py/c-Al_2O_3 (sample A), Py/n-GaN:Si (sample E), and Py/u-GaN (sample B) are shown in Fig. 2(a), where u-GaN is an unintentionally doped GaN layer with thickness 1.0 μm and carrier concentration $\sim(3.0\times10^{16})$ cm^{-3}. The difference in broadening of the linewidth between the Py/n-GaN:Si bilayer and the Py layer, i.e., $[\Delta H_{pp}^{||}(\text{Py}/n\text{:GaN:Si}) - \Delta H_{pp}^{||}(\text{Py})]$, is $\sim$2.87 mT, while the one for the Py/u-GaN bilayer and Py, i.e., $[\Delta H_{pp}^{||}(\text{Py}/u\text{-GaN}) - \Delta H_{pp}^{||}(\text{Py})]$, is estimated to be 0.2 mT. By measuring the FMR for in-plane and for out-of-plane orientations of the magnetic fields and estimating the linewidths, information on the physical origin of the damping parameter α can be gained. We measure the in-plane and out-of-plane FMR for a Py/n-GaN:Si (sample C) and the data are reported in Fig. 2(b). The intensity of the FMR absorption for the out-of-plane ($\theta_H = 90°$) is significantly reduced and the line shape is found to be asymmetric. By comparing the linewidths for these two orientations we see that $\Delta H_{pp}^{||} \leqslant \Delta H_{pp}^{\perp}$ indicating an intrinsic Gilbert damping along with inhomogeneous broadening due to the sample inhomogeneities arising from the polycrystalline nature of the deposited Py film [58]. To investigate the nature of the Py/u-GaN and Py/n-GaN:Si interfaces, I-V characteristics for samples B and C have been recorded over a broad range of temperatures and the data are given in Figs. 2(c) and 2(d). The Py/n-GaN:Si interface behaves as an Ohmic contact, while for the Py/u-GaN a Schottky barrier with a depletion layer is observed, which persists up to the RT. It has been already established that a Schottky barrier inhibits spin pumping in semiconductors [59] and in the present study no spin-pumping-induced emf V_H is detected for sample B with a Schottky behavior.

The dynamics of the magnetization $\vec{M}(t)$ in Py under an effective magnetic field $\vec{H}_{eff}$ is described by the LLG Eq. (1). In FMR regime, the spin pumping driven by dynamical exchange interaction pumps into n-GaN:Si pure spin current, which gets converted into charge current via ISHE, according to the relation $\vec{J}_c = \theta_{SH}\vec{J}_s \times \vec{\sigma}$, as discussed earlier. The charge current in the Rashba semiconductor leads to an emf proportional to the generated spin current and whose amplitude is proportional to the microwave absorption and maximized at the resonance field H_{FMR}.

The emf V_H generated in the NM n-GaN:Si (sample C) is detected simultaneously with the FMR and at the resonance field a peak is observed in the measured voltage. The experimental emf is plotted as a function of the applied magnetic field $\vec{H}$ and reported in Figs. 3(a) and 3(b) respectively for $\theta_H = 0°$ and $\theta_H = 180°$. The angles 0° and 180° define the directions of the magnetic field applied in-plane in accordance to the geometry provided in Fig. 1(c). Since the Rashba-Edelstein effect is observed in 2DEGs and in materials with giant Rashba SOC [60], and given that the system treated here belongs to neither of these two classes, the observed emf is attributed to the interplay between SHE and ISHE. The experimental emf V_H is a superposition of the voltage due to ISHE in the n-GaN:Si layer [26,59] and of spurious voltages originating from galvanomagnetic effects such as the ordinary Hall effect (OHE) in n-GaN:Si, anomalous Hall effect (AHE), planar Hall effect (PHE) in the Py layer, and thermal heating effects due to microwave irradiation [61]. The voltage originating from these spurious mechanisms can be separated from the one due

to ISHE by fitting the experimental data with the function [26]

$$V_H = V_{Sym}\frac{\Gamma^2}{(H-H_{FMR})^2+\Gamma^2} + V_{Asym}\frac{-2\Gamma(H-H_{FMR})}{(H-H_{FMR})^2+\Gamma^2}, \quad (2)$$

where Γ is the half linewidth of the FMR line shape and H_{FMR} is the resonance field. The symmetric part of the total voltage function, $V_{Sym}\Gamma^2/[(H-H_{FMR})^2+\Gamma^2]$, with an absorption line shape is the contribution of the ISHE voltage V_{ISHE} developed in n-GaN:Si due to the adiabatic spin pumping and to heating effects. On the other hand, the asymmetric part of the function, $V_{Asym}[-2\Gamma(H-H_{FMR})]/[(H-H_{FMR})^2+\Gamma^2]$ with a dysonian dispersion line shape is a consequence of the contributions from AHE and OHE, as discussed earlier. The Hall voltages V_{Asym} change sign across H_{FMR}, while V_{ISHE}—being proportional to the integrated microwave absorption intensity—is symmetric across H_{FMR}, as expected from the fundamental spin pumping model [25,26]. A fitting of the measured emf at a microwave power of 200 mW with Eq. (2) for $\theta_H = 0^\circ$ yields $V_{Sym} = 2.80\ \mu$V and $V_{Asym} = -0.453\ \mu$V. The ratio $V_{Sym}/V_{Asym}\sim 6$ indicates that the major contribution to the measured voltage is provided by the efficient conversion of spin-to-charge current due to an interplay of spin pumping and direct-and-inverse spin Hall effects. The spurious heating effects from the microwave irradiation can be further eliminated by averaging the symmetric voltage for parallel and antiparallel orientation of the applied field H according to

$$V_{ISHE}(\theta_H) = \frac{V_{Sym}(\theta_H) - V_{Sym}(\theta_H+180^\circ)}{2}. \quad (3)$$

This approach to the treatment of the data is justified, since V_{ISHE} changes sign upon reversal of the magnetic field owing to a change of sign of the spin polarization vector $\vec{\sigma}$, not occurring for the voltage due to the microwave heating effects. Thus, for spin pumping experiments, the measured emf V_H includes contributions from both symmetric and asymmetric voltages, and the actual ISHE voltage V_{ISHE} is estimated by a proper treatment of the measured data. It was reported [30,36,62,63] that the symmetric voltage can also include contributions from PHE and galvanomagnetic effects in the metallic FM layer due to the electric and magnetic field components of the microwave. However, the angular dependence of the emf with respect to the external magnetic field showed that the contribution of the ISHE to the symmetric voltages is at least five times greater than the ones from the PHE [63]. Considering a spherical Fermi surface at the FM/NM interface, the enhanced Gilbert damping parameter $\Delta\alpha$ is related to the spin diffusion length λ_N and thickness d_N of the NM as [64,65]

$$\Delta\alpha = \frac{\gamma\hbar g_r^{\uparrow\downarrow}}{4\pi M_s d_{FM}}(1-e^{-2d_N/\lambda_N}), \quad (4)$$

where d_F is the thickness of the FM layer. Using Eq. (4) and estimating the enhanced α for Py/n-GaN:Si bilayers as a function of d_N we estimate a spin diffusion length $\lambda_N \sim 77$ nm in the n-GaN:Si layers at RT, which agrees with the one reported by Jahangir *et al.* [66].

In the above mentioned works [30,36,62,63], the thickness of the NM layer was of the order of the spin diffusion length λ_N, while the thicknesses of the n-GaN:Si films studied here is $\sim$1.0 μm, i.e., much greater than the spin diffusion length $\lambda_N \sim 77$ nm in n-GaN:Si. The fact that the thickness of the NM is orders of magnitude greater than λ_N suppresses the backflow spin current into the metallic FM, further reducing the contributions to the emf from galvanomagnetic effects. Careful identification and estimation of the various components of the emf generated in the NM layer in a spin pumping experiment is therefore essential for the estimation of the spin-to-charge conversion efficiency of a material. Here, for the in-plane magnetic field, after eliminating the heating effects, a $V_{ISHE} = 3.25\ \mu$V is obtained and is exploited for the quantitative evaluation of the spin Hall angle for n-GaN:Si.

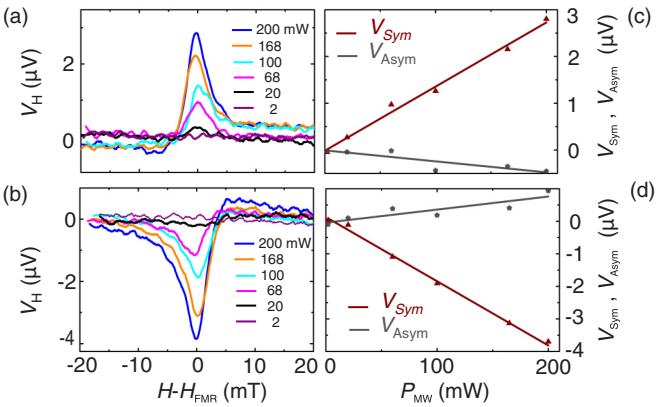

FIG. 4. Dependence of the measured voltage on the applied microwave power for in-plane magnetic field orientations at (a) $\theta_H = 0^\circ$ and (b) $\theta_H = 180^\circ$. Dependence of the V_{Sym} and V_{Asym} for different microwave powers for (c) $\theta_H = 0^\circ$ and (d) $\theta_H = 180^\circ$.

The dependence of the measured emf on the applied microwave power under FMR conditions is shown in Figs. 4(a) and 4(b) for orientations of the magnetic field $\theta_H = 0^\circ$ and $\theta_H = 180^\circ$, respectively. For a microwave power of 200 mW, the measured voltages at FMR conditions are $+2.849\ \mu$V for $\theta_H = 0^\circ$ and $-3.840\ \mu$V for $\theta_H = 180^\circ$. It is to be noted here that the voltages reported in Figs. 4(a) and 4(b) contain both the symmetric and asymmetric contributions. After separating the symmetric and asymmetric voltage components, the symmetric part of the voltage, V_{Sym}, is plotted as a function of P_{MW} and shown in Figs. 4(c) and 4(d) for $\theta_H = 0^\circ$ and $\theta_H = 180^\circ$, respectively. Now, being V_{ISHE} proportional to the square of the microwave magnetic field (h_{MW}), it is expected to be linearly proportional to the microwave power P_{MW} [39,59]. This is validated in Figs. 4(c) and 4(d) for $\theta_H = 0^\circ$ and $\theta_H = 180^\circ$, respectively. The reversal of $\vec{H}$ causes $\vec{\sigma}$ to change sign, which in turn induces the change in sign of the ISHE electric field $\vec{E}_{ISHE}$, as evidenced in Figs. 4(a) and 4(b). It can be concluded that the fundamental relation for the ISHE, $\vec{J}_c = \theta_{SH}\vec{J}_s \times \vec{\sigma}$, operates in the studied Py/n-GaN:Si bilayer system. For an applied magnetic field perpendicular to the sample plane, i.e., $\theta_H = 90^\circ$, the amplitude of V_{ISHE} is quenched even though a FMR signal for the Py is detected at the resonance field of 1245 mT. This result provides the necessary and sufficient confirmation of spin pumping through SHE and ISHE in n-GaN:Si.

IV. ESTIMATION OF SPIN HALL ANGLE IN *n*-GaN:Si

The magnetization precession described by the LLG Eq. (1) drives the spin pumping mechanism in the Py/*n*-GaN:Si film. Within the fundamental model of spin pumping proposed by Tserkovnyak *et al.* [21], the dc component of the generated spin current density j_s^0 at the interface between Py and *n*-GaN:Si is

$$j_s^0 = \frac{\omega}{2\pi}\int_0^{2\pi}\frac{\hbar}{4\pi}g_r^{\uparrow\downarrow}\frac{1}{M_s^2}\left[\vec{M}(t)\times\frac{d\vec{M}(t)}{dt}\right]_z dt, \quad (5)$$

where $\hbar$ and $g_r^{\uparrow\downarrow}$ are the Dirac constant and real part of the spin mixing conductance, while $[\vec{M}(t)\times d\vec{M}(t)/dt]_z$ is the z component of $[\vec{M}(t)\times d\vec{M}(t)/dt]$. Now, $g_r^{\uparrow\downarrow}$ is proportional to the reflection and transmission coefficients of the majority and minority spins of the NM electrons, which in turn depend on the transparency of the FM/NM interface [67,68]. Thus, a transparent interface, i.e., one with negligible spin scattering potential centers, would enhance $g_r^{\uparrow\downarrow}$ by augmenting the spin current density in the NM. The resonance condition obtained as a solution of the LLG equation is given by

$$\left(\frac{\omega}{\gamma}\right)^2 = H_{\rm FMR}(H_{\rm FMR}+4\pi M_s), \quad (6)$$

where $H_{\rm FMR}$ is the resonance field, ω the frequency of the microwave radiation, and γ is the gyromagnetic ratio. Using Eqs. (5) and (6) and the dynamic components of the magnetization $\vec{M}(t)$ obtained as a solution of Eq. (1) with the components of $\vec{H}_{\rm eff}$ as discussed above [28], the spin current density j_s^0 is

$$j_s^0 = \frac{g_r^{\uparrow\downarrow}\gamma^2 h_{MW}^2\hbar[4\pi M_s\gamma+\sqrt{(4\pi M_s)^2\gamma^2+4\omega^2}]}{8\pi\alpha^2[(4\pi M_s)^2\gamma^2+4\omega^2]}. \quad (7)$$

The spin Hall angle $\theta_{\rm SH}$ is related to the spin current j_s^0 and to the inverse spin Hall voltage $V_{\rm ISHE}$ as

$$\theta_{\rm SH} = \left(\frac{\hbar}{2e}\right)\frac{V_{\rm ISHE}(d_N\sigma_N+d_F\sigma_F)}{w\sigma_N\tanh\left(\frac{d_N}{2\lambda_N}\right)j_s^0}, \quad (8)$$

where $d_{\rm N}$, $\sigma_{\rm N}$, and $\lambda_{\rm N}$ are the thickness, conductivity, and spin diffusion length of the *n*-GaN:Si layer, respectively, while $d_{\rm F}$ and $\sigma_{\rm F}$ are the thickness and conductivity of the ferromagnet Py. The real part of the spin mixing conductance $g_r^{\uparrow\downarrow}$ is given by [25,28,29,69]

$$g_r^{\uparrow\downarrow} = \frac{4\pi M_s\sqrt{3}\gamma d_{\rm F}}{2g\mu_B\mu_0\omega}[\Delta H_{\rm pp}^{||}({\rm FM/NM})-\Delta H_{\rm pp}^{||}({\rm FM})], \quad (9)$$

where g and $\mu_{\rm B}$ are the Landé g factor and the Bohr magneton, and $\Delta H_{\rm pp}^{||}$(FM/NM) and $\Delta H_{\rm pp}^{||}$(FM) the spectral linewidths of the Py/GaN:Si and Py layers, as shown in Fig. 1(d). For sample C with $g=2.12$, $4\pi M_{\rm s}=0.938$ T, $d_{\rm F}=(1\times10^{-8})$ m, $\mu_B=(9.27\times10^{-24})$ J T^{-1}, $\omega=(5.931\times10^{10})$ s^{-1}, and $\mu_0=(4\pi\times10^{-7})$ H/m, we calculate the spin mixing conductance $g_r^{\uparrow\downarrow}$ to be (1.38×10^{18}) m^{-2}. Using Eqs. (6) and (7) and with the parameters $\gamma=(1.86\times10^{11})$ T^{-1} s^{-1}, $h_{\rm MW}=0.15$ mT, $\hbar=(1.054\times10^{-34})$ J s, $\lambda_{\rm N}=77$ nm, $d_{\rm N}=1.9$ μm, $w=3$ mm, $d_{\rm F}=10$ nm, $\sigma_{\rm N}=(3.5587\times10^4)$ Ω^{-1} m^{-1}, $\sigma_F=(1.6\times10^6)$ Ω^{-1} m^{-1}, $j_s^0=(1.2254\times10^{-10})$ J m^{-2}, and $V_{\rm ISHE}=3.25$ μV, we find the spin Hall angle for *n*-GaN:Si to be $\theta_{\rm SH}=3.03\times10^{-3}$, at least one order of magnitude higher than those reported for Si [38], Ge [70], ZnO [41], and *n*-GaAs [6,71]. The spin Hall angle $\theta_{\rm SH}$ depends on both the side jump and the skew scattering mechanisms. Theoretically [29] the side jump contribution to $\theta_{\rm SH}$ is given by $(3/8)^{1/2}(k_{\rm F}\lambda_{\rm N})^{-1}$, which corresponds to 1.08×10^{-2} in the case under consideration. The theoretical value is at least one order of magnitude higher than the one obtained experimentally. By defining the evolution of SHE in terms of mobility of the system in question according to Vignale *et al.* [17], with $\mu\sim180$ cm^2 V^{-1} s^{-1}, *n*-GaN:Si falls in the limit of the clean-ultraclean regime, which is dominated by the skew scattering. Considering the above mentioned overestimation of the magnitude of the side jump contribution and the consequent discrepancy between the theoretical and experimental values of $\theta_{\rm SH}$, one can infer that SHE in *n*-GaN:Si is dominated by skew scattering.

V. THICKNESS-DEPENDENT SPIN PUMPING IN *n*-GaN:Si

The experiments discussed above for the 1.9 μm thick *n*-GaN:Si layer have been carried out also on a series of samples with thickness of the *n*-GaN:Si film between 150 nm and 1.7 μm (samples D to H). Like in the case of the 1.9 μm *n*-GaN:Si sample, an AlO_x passivated 10 nm Py film is used as the source of spin. The spin Hall voltage measured in the 150-nm-thick *n*-GaN:Si (sample H) is reported in Fig. 5. Here, the intensity of the asymmetric component of the voltage is more than one order of magnitude higher than the one observed for the 1.9 μm *n*-GaN:Si sample, as shown in Figs. 5(a) and 5(b).

By taking into account that only the electrons at the Fermi surface participate in the spin pumping, the forward spin current $I_{\rm sp}$ and the spin backflow current can be related as $I_{\rm bf}=I_{\rm sp}\exp(-2d_{\rm N}/\lambda_{\rm N})$ [64]. Thus, for *n*-GaN:Si layers with $d_{\rm N}\approx\lambda_{\rm N}$, the spin backflow current is expected to dominate. In fact as described later, we do observe the influence of $d_{\rm N}$ on the estimated $\theta_{\rm H}$ of *n*-GaN:Si. For a NM layer thinner than its $\lambda_{\rm N}$, $I_{\rm bf}$ from the NM to FM exceeds $I_{\rm sp}$ due to spin pumping [25,64,72]. In such a scenario, because of inverse spin Hall effect $V_{\rm ISHE}$ cannot be detected in the NM. However, the asymmetric voltages can still be seen, being independent of spin pumping. In the present case of *n*-GaN:Si we have found the spin diffusion length to be $\lambda_{\rm N}\sim77$ nm. It was reported that for NM metal systems, the asymmetry voltage contribution for a film thickness of the order of $\lambda_{\rm N}$ is close to 100% of the total emf measured. This is due to the dominance of $I_{\rm bf}$ over $I_{\rm sp}$ [73]. However, with a greater thickness of the NM film, the asymmetric contribution diminishes and approaches a minimum saturation value for a film thickness $\gg\lambda_{\rm N}$. Furthermore, it was reported by Flovik *et al.* [74] that this significant $V_{\rm Asym}$ could be assigned to Eddy current effects and it was shown that in the case of a NM Pt layer, the asymmetry decreases considerably with increasing the thickness of the NM layer. In the systems considered here, for thin layers of *n*-GaN:Si the spin backflow is likely to be the dominant mechanism that leads to the suppression of the $V_{\rm Sym}$ signal, since the Oersted fields induce a significant distortion of the FMR line shape, not observed for the 1.9-μm-thick *n*-GaN:Si sample. For the case of ZnO—also a wide band gap wurtzite semiconductor such as GaN—D'Ambrosio *et al.* [40]

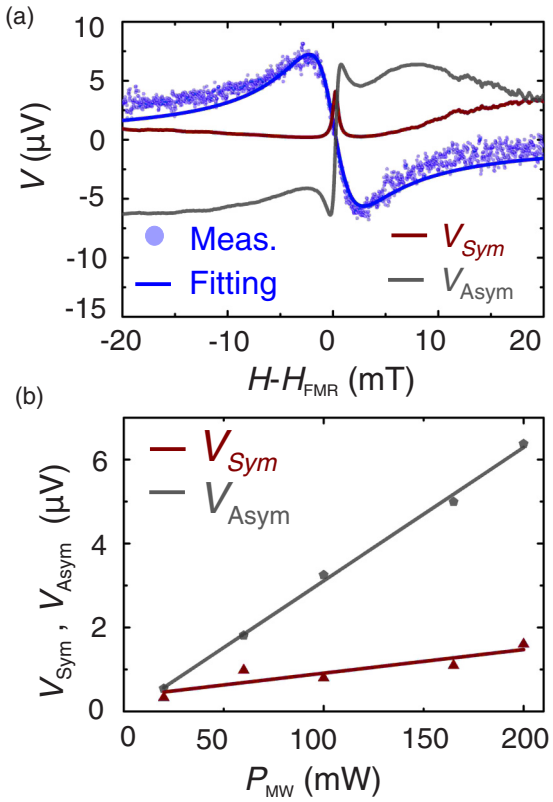

FIG. 5. (a) Voltage across the electrodes in the 150 nm n-GaN:Si control sample under a microwave excitation of power 200 mW. Dots: experimental data; solid lines: fitting according to Eq. (2). (b) Measured V_{ISHE} and V_{Asym} as a function of the microwave power. Lines: linear fits.

reported the measured emf from the ZnO layer in a Py/ZnO bilayer under FMR conditions, as due to PHE in the Py film. In our case of n-GaN:Si, the control experiments—as previously mentioned—did not reveal any measurable voltage due to PHE in the Py layer. Moreover, the thickness of the ZnO film used in case of D'Ambrosio *et al.* was 200 nm, making spin backflow a likely reason for the observed dominant contribution from PHE. On the other hand, in our case for calculating the spin Hall angle θ_{SH} we carry out measurements on a 1.9-μm-thick n-GaN:Si layer, which can be considered as a bulk system where the role of spin backflow is largely suppressed—as discussed previously in detail—upon comparison with the 150 nm n-GaN:Si layer.

In a linear response regime, both V_{Sym} and V_{Asym} have the same power dependence, and the spectral weight of the asymmetric component, β, can be expressed as

$$\beta = \frac{1}{1 + |V_{\mathrm{Sym}}/V_{\mathrm{Asym}}|}. \tag{10}$$

The variation of β as a function of the n-GaN:Si thickness d_{N} is reported in Fig. 6(a). For $d_{\mathrm{N}} = 150$ nm (sample H), $\beta \sim 0.9$ while for samples with $d_{\mathrm{N}} \geqslant 150$ nm (samples C, D, E, and F) β decreases with increasing n-GaN:Si layer thickness until it reaches a saturation value $\sim$0.2 for $d_{\mathrm{N}} \geqslant 1.0$ μm. The theoretical value of β for a single Py layer is $\sim$1, indicating the presence of an exclusive asymmetric component due to the

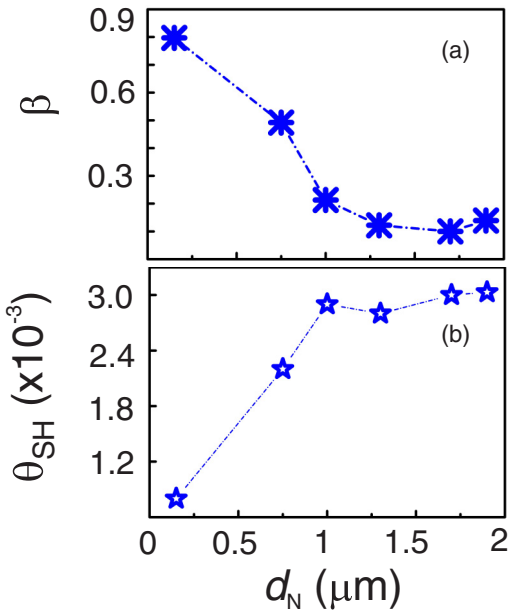

FIG. 6. Variation of estimated values for (a) β and (b) θ_{SH} as a function of the n-GaN:Si thickness d_{N}.

PHE in the ferromagnetic layer. The spin Hall angles θ_{SH} as a function of d_{N} are reported in Fig. 6(b) and identical values of θ_{SH} are estimated for samples with thicknesses $d_{\mathrm{N}} \geqslant 1$ μm. For sample G ($d_{\mathrm{N}} = 750$ nm), θ_{SH} is smaller than the one of the thicker samples, while it is almost one order of magnitude lower for sample H, with the lowest thickness. The observed behavior of β indicates that in order to have efficient spin-to-charge conversion in the Rashba semiconductor n-GaN:Si, the NM layer must be chosen to be much greater than the spin diffusion length λ_{N}. Such behavior for β has been reported for Pd [65] though the length scale for the metallic system of Pd is orders of magnitude lower than the one for the present system of degenerate n-GaN:Si.

Another important aspect of III-nitride heteroepitaxial crystals is the presence of threading dislocations [75]. By virtue of their wide band gaps and non-negligible RSOC, the electron spin coherence in the n-GaN:Si films treated here yields high spin lifetimes $\sim$20 ns persisting up to room temperature, despite the presence of $\sim 5\times10^{8}$ cm^{-2} charged threading dislocations. The charged dislocations might also induce side jump mechanisms alongside the skew scattering, thereby contributing to the value found for θ_{SH} compared to other semiconducting systems. Tuning the threading dislocation densities using a homoepitaxial growth of the n-GaN:Si on freestanding GaN substrates can give quantitative insights into the role of dislocations in extrinsic spin Hall effects in wurtzite GaN systems.

VI. LOW-TEMPERATURE DEPENDENCY OF SPIN PUMPING IN n-GaN:Si

Low-temperature spin pumping measurements have been carried out on samples A, C, and E over the temperature range 4 K $\leqslant T \leqslant$ 300 K, but no detectable voltage V_{H} could be measured for $T \leqslant 275$ K. With the employed experimental

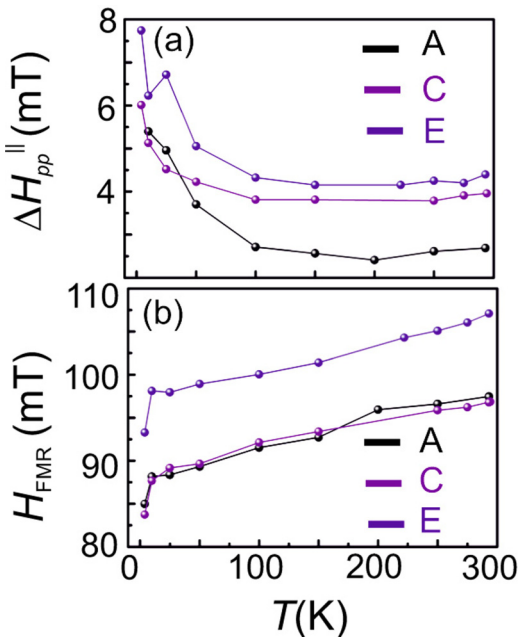

FIG. 7. (a) FMR linewidth $\Delta H_{pp}^{||}$ and (b) resonance field H_{FMR} for samples A, C, and E measured as a function of temperature.

setup we are not able to detect any spin-pumping-induced emf for temperatures below RT. While the presence of low-temperature spin pumping cannot be ruled out, the related emf might be below the sensitivity of the instruments. Significant reduction of spin pumping efficiency has been recently reported in Pt/YIG-based bilayers [76], where an increase in the Gilbert damping parameter was identified as the dominant factor in the observed quenching of the V_{ISHE}. The linewidth of the FMR spectra for an applied in-plane magnetic field $\Delta H_{pp}^{||}$ and the resonance field H_{FMR} as a function of temperature are reported in Figs. 7(a) and 7(b), respectively.

An increase in $\Delta H_{pp}^{||}$ with decreasing temperature is observed, indicating an increment of the Gilbert damping parameter α. On the other hand, H_{FMR} is found to monotonically decrease with decreasing temperature with a sudden dip below 10 K. The slightly higher H_{FMR} for sample E is caused by an unintentional shift in the X-band frequency to a higher value due to the electronics in the microwave bridge during the FMR measurements. Such a behavior of H_{FMR} as a function of temperature points to the presence of a thin native oxide layer on Py [77]. From XPS measurements, as shown in the Supplemental Material [57], native oxides of Fe are detected at the AlO_x/Py interface and this explains the observed dependence of H_{FMR} on temperature. From spin pumping theory [21] it is appreciated that in a diffusive FM/NM bilayer any change in α is caused by the spin mixing conductance $g_r^{\uparrow\downarrow}$ due to the transfer of spin angular momentum from the FM to the NM layer at resonance conditions. For the system studied here, $g_r^{\uparrow\downarrow}$ is controlled by the conductivity $\sigma(T)$ of the n-GaN:Si. Being a degenerate semiconductor, n-GaN:Si exhibits a temperature-independent electrical conductivity [54], as seen from Fig. 2(c) for the Py/n-GaN:Si interface. However, the absence of a detectable emf due to the ISHE despite the enhanced α might be related to defect states at the Py/n-GaN:Si interface, which modify the transparency for the injected spin current, causing an enhanced backflow of spins into the Py.

VII. CONCLUSIONS

We have provided experimental demonstration of spin-pumping-induced spin current generation and its detection at room temperature using the ISHE in the Rashba semiconductor n-GaN:Si. From the fundamental model of spin pumping, a spin mixing conductance of (1.38×10^{18}) m^{-2} for the Py/n-GaN:Si interface and a spin Hall angle $\theta_{SH} = 3.03\times10^{-3}$ for wz n-GaN:Si with thicknesses $\geqslant 1.0$ μm are found. We also demonstrate the importance of thickness of the NM layer for efficient spin pumping in diffusive FM/NM bilayer systems. The value obtained for θ_{SH} is at least one order of magnitude higher than those of other semiconductors such as Si, Ge, ZnO, and n-GaAs. The spin pumping is found to quench at low temperatures. The experimental demonstration of generation of pure spin current in n-GaN:Si and its enhanced spin-to-charge conversion efficiency over other functional semiconductors points to III-nitrides as model systems for studies on spin-related phenomena in noncentrosymmetric semiconductors. Moreover, this work paves the way to the realization of nitride-based low-power optoelectronic, nonvolatile, and low-dissipative spin devices such as spin batteries.

ACKNOWLEDGMENTS

This work was supported by the FunDMS Advanced Grant of the European Research Council (ERC Grant No. 227690), by the Austrian Science Foundation–FWF (P22477, P24471, and P26830), by the NATO Science for Peace Programme (Project No. 984735), and by the EU 7th Framework Programmes: CAPACITIES project REGPOT-CT-2013-316014 (EAgLE) and the EU Horizon 2020 Research and Innovation Programme (Grant No. 645776). The authors would also like to acknowledge the experimental support for SQUID magnetometry by M. Sawicki, Institute of Physics, Polish Academy of Sciences, Warsaw, Poland.

[1] A. Hoffmann and S. D. Bader, Phys. Rev. Appl. **4**, 047001 (2015).
[2] T. Kuschel and G. Reiss, Nat. Nanotechnol. **10**, 22 (2015).
[3] W. Zhang, M. B. Jungfleisch, W. Jiang, J. Sklenar, F. Y. Fradin, J. E. Pearson, J. B. Ketterson, and A. Hoffmann, J. Appl. Phys. **117**, 172610 (2015).
[4] A. Manchon, Nat. Phys. **10**, 340 (2014).
[5] A. Fert, V. Cros, and J. Sampaio, Nat. Nanotechnol. **8**, 152 (2013).
[6] J. Sinova, S. O. Valenzuela, J. Wunderlich, C. H. Back, and T. Jungwirth, Rev. Mod. Phys. **87**, 1213 (2015).
[7] V. Edelstein, Solid State Commun. **73**, 233 (1990).

[8] G. Vignale and I. V. Tokatly, Phys. Rev. B **93**, 035310 (2016).
[9] N. Nagaosa, J. Sinova, S. Onoda, A. H. MacDonald, and N. P. Ong, Rev. Mod. Phys. **82**, 1539 (2010).
[10] N. F. Mott, Proc. R. Soc. A **124**, 425 (1929).
[11] M. I. D'yakonov and V. I. Perel', JETP Lett. **13**, 467 (1971).
[12] J. E. Hirsch, Phys. Rev. Lett. **83**, 1834 (1999).
[13] S. Zhang, Phys. Rev. Lett. **85**, 393 (2000).
[14] J. Sinova, D. Culcer, Q. Niu, N. A. Sinitsyn, T. Jungwirth, and A. H. MacDonald, Phys. Rev. Lett. **92**, 126603 (2004).
[15] S. Murakami, N. Nagaosa, and S.-C. Zhang, Science **301**, 1348 (2003).
[16] S. Murakami, in *Advances in Solid State Physics*, edited by B. Kramer (Springer, Berlin, 2006), Vol. 45, pp. 197-209.
[17] G. Vignale, J. Supercond. Novel Magn. **23**, 3 (2009).
[18] Y. K. Kato, R. C. Myers, A. C. Gossard, and D. D. Awschalom, Science **306**, 1910 (2004).
[19] J. Wunderlich, B. Kaestner, J. Sinova, and T. Jungwirth, Phys. Rev. Lett. **94**, 047204 (2005).
[20] T. Jungwirth, J. Wunderlich, and K. Olejnik, Nat. Mater. **11**, 382 (2012).
[21] Y. Tserkovnyak, A. Brataas, and G. E. W. Bauer, Phys. Rev. Lett. **88**, 117601 (2002).
[22] Y. Tserkovnyak, A. Brataas, and G. E. W. Bauer, Phys. Rev. B **66**, 224403 (2002).
[23] A. Brataas, Y. Tserkovnyak, G. E. W. Bauer, and B. I. Halperin, Phys. Rev. B **66**, 060404 (2002).
[24] K. Ando, Semicond. Sci. Technol. **29**, 043002 (2014).
[25] Y. Tserkovnyak, A. Brataas, G. E. W. Bauer, and B. I. Halperin, Rev. Mod. Phys. **77**, 1375 (2005).
[26] E. Saitoh, M. Ueda, H. Miyajima, and G. Tatara, Appl. Phys. Lett. **88**, 182509 (2006).
[27] Y. Pu, P. M. Odenthal, R. Adur, J. Beardsley, A. G. Swartz, D. V. Pelekhov, M. E. Flatté, R. K. Kawakami, J. Pelz, P. C. Hammel, and E. Johnston-Halperin, Phys. Rev. Lett. **115**, 246602 (2015).
[28] K. Ando, Y. Kajiwara, S. Takahashi, S. Maekawa, K. Takemoto, M. Takatsu, and E. Saitoh, Phys. Rev. B **78**, 014413 (2008).
[29] K. Ando, S. Takahashi, J. Ieda, Y. Kajiwara, H. Nakayama, T. Yoshino, K. Harii, Y. Fujikawa, M. Matsuo, S. Maekawa, and E. Saitoh, J. Appl. Phys. **109**, 103913 (2011).
[30] A. Azevedo, L. H. Vilela-Leão, R. L. Rodríguez-Suárez, A. F. Lacerda Santos, and S. M. Rezende, Phys. Rev. B **83**, 144402 (2011).
[31] C. T. Boone, J. M. Shaw, H. T. Nembach, and T. J. Silva, J. Appl. Phys. **117**, 223910 (2015).
[32] G. Allen, S. Manipatruni, D. E. Nikonov, M. Doczy, and I. A. Young, Phys. Rev. B **91**, 144412 (2015).
[33] C. O. Avci, K. Garello, C. Nistor, S. Godey, B. Ballesteros, A. Mugarza, A. Barla, M. Valvidares, E. Pellegrin, A. Ghosh, I. M. Miron, O. Boulle, S. Auffret, G. Gaudin, and P. Gambardella, Phys. Rev. B **89**, 214419 (2014).
[34] Y. Ando, K. Ichiba, S. Yamada, E. Shikoh, T. Shinjo, K. Hamaya, and M. Shiraishi, Phys. Rev. B **88**, 140406 (2013).
[35] B. Heinrich, C. Burrowes, E. Montoya, B. Kardasz, E. Girt, Y.-Y. Song, Y. Sun, and M. Wu, Phys. Rev. Lett. **107**, 066604 (2011).
[36] L. Chen, F. Matsukura, and H. Ohno, Nat. Commun. **4**, 2055 (2013).
[37] C. Liu, S. J. Patel, T. A. Peterson, C. C. Geppert, K. D. Christie, G. Stecklein, C. J. Palmstrom, and P. A. Crowell, Nat. Commun. **7**, 10296 (2016).
[38] K. Ando and E. Saitoh, Nat. Commun. **3**, 629 (2012).
[39] S. Dushenko, M. Koike, Y. Ando, T. Shinjo, M. Myronov, and M. Shiraishi, Phys. Rev. Lett. **114**, 196602 (2015).
[40] S. D'Ambrosio, L. Chen, H. Nakayama, F. Matsukura, T. Dietl, and H. Ohno, Jpn. J. Appl. Phys. **54**, 093001 (2015).
[41] J.-C. Lee, L.-W. Huang, D.-S. Hung, T.-H. Chiang, J. C. A. Huang, J.-Z. Liang, and S.-F. Lee, Appl. Phys. Lett. **104**, 052401 (2014).
[42] M. Jamali, J. S. Lee, J. S. Jeong, F. Mahfouzi, Y. Lv, Z. Zhao, B. K. Nikolić, K. A. Mkhoyan, N. Samarth, and J.-P. Wang, Nano Lett. **15**, 7126 (2015).
[43] C. Rinaldi, J. C. Rojas-Sánchez, R. N. Wang, Y. Fu, S. Oyarzun, L. Vila, S. Bertoli, M. Asa, L. Baldrati, M. Cantoni, J.-M. George, R. Calarco, A. Fert, and R. Bertacco, APL Mater. **4**, 032501 (2016).
[44] Y. Kajiwara, K. Harii, S. Takahashi, J. Ohe, K. Uchida, M. Mizuguchi, H. Umezawa, H. Kawai, K. Ando, K. Takanashi, S. Maekawa, and E. Saitoh, Nature (London) **464**, 262 (2010).
[45] C. W. Sandweg, Y. Kajiwara, A. V. Chumak, A. A. Serga, V. I. Vasyuchka, M. B. Jungfleisch, E. Saitoh, and B. Hillebrands, Phys. Rev. Lett. **106**, 216601 (2011).
[46] L. J. Cornelissen, J. Liu, R. A. Duine, J. B. Youssef, and B. J. van Wees, Nat. Phys. **11**, 1022 (2015).
[47] Y. Shiomi and E. Saitoh, Phys. Rev. Lett. **113**, 266602 (2014).
[48] L. Frangou, S. Oyarzún, S. Auffret, L. Vila, S. Gambarelli, and V. Baltz, Phys. Rev. Lett. **116**, 077203 (2016).
[49] R. Cheng, J. Xiao, Q. Niu, and A. Brataas, Phys. Rev. Lett. **113**, 057601 (2014).
[50] A. Bonanni, M. Sawicki, T. Devillers, W. Stefanowicz, B. Faina, T. Li, T. E. Winkler, D. Sztenkiel, A. Navarro-Quezada, M. Rovezzi, R. Jakieła, A. Grois, M. Wegscheider, W. Jantsch, J. Suffczyński, F. D'Acapito, A. Meingast, G. Kothleitner, and T. Dietl, Phys. Rev. B **84**, 035206 (2011).
[51] T. Dietl, K. Sato, T. Fukushima, A. Bonanni, M. Jamet, A. Barski, S. Kuroda, M. Tanaka, P. N. Hai, and H. Katayama-Yoshida, Rev. Mod. Phys. **87**, 1311 (2015).
[52] E. I. Rashba, Fiz. Tverd. Tela **2**, 1224 (1960).
[53] E. I. Rashba, Sov. Phys. Usp. **7**, 823 (1965).
[54] W. Stefanowicz, R. Adhikari, T. Andrearczyk, B. Faina, M. Sawicki, J. A. Majewski, T. Dietl, and A. Bonanni, Phys. Rev. B **89**, 205201 (2014).
[55] H. Nakayama, K. Ando, K. Harii, T. Yoshino, R. Takahashi, Y. Kajiwara, K. Uchida, Y. Fujikawa, and E. Saitoh, Phys. Rev. B **85**, 144408 (2012).
[56] S.-I. Kim, M.-S. Seo, J.-H. Seo, H. J. Yun, J. Lee, Y. S. Choi, and S. Young Park, Curr. Appl. Phys. **14**, 1743 (2014).
[57] See Supplemental Material at http://link.aps.org/supplemental/10.1103/PhysRevB.94.085205 for details on XPS measurements at the interface AlO_x/Py.
[58] T. G. A. Verhagen, H. N. Tinkey, H. C. Overweg, M. van Son, M. Huber, J. M. van Ruitenbeek, and J. Aarts, J. Phys.: Condens. Matter **28**, 056004 (2016).
[59] K. Ando, S. Takahashi, J. Ieda, H. Kurebayashi, T. Trypiniotis, C. H. W. Barnes, S. Maekawa, and E. Saitoh, Nat. Mater. **10**, 655 (2011).
[60] J.-C. Rojas-Sánchez, L. Vila, G. Desfonds, S. Gambarelli, J. P. Attané, J. M. De Teresa, C. Magén, and A. Fert, Nat. Commun. **4**, 2944 (2013).
[61] H. J. Juretschke, J. Appl. Phys. **31**, 1401 (1960).
[62] L. Chen, S. Ikeda, F. Matsukura, and H. Ohno, Appl. Phys. Express **7**, 013002 (2014).

[63] J. Lustikova, Y. Shiomi, and E. Saitoh, Phys. Rev. B **92**, 224436 (2015).
[64] J. Foros, G. Woltersdorf, B. Heinrich, and A. Brataas, J. Appl. Phys. **97**, 10A714 (2005).
[65] J. M. Shaw, H. T. Nembach, and T. J. Silva, Phys. Rev. B **85**, 054412 (2012).
[66] S. Jahangir, F. Doğan, H. Kum, A. Manchon, and P. Bhattacharya, Phys. Rev. B **86**, 035315 (2012).
[67] W. Zhang, W. Han, X. Jiang, S.-H. Yang, and S. S. P. Parkin, Nat. Phys. **11**, 496 (2015).
[68] C.-F. Pai, Y. Ou, L. H. Vilela-Leão, D. C. Ralph, and R. A. Buhrman, Phys. Rev. B **92**, 064426 (2015).
[69] P. Deorani and H. Yang, Appl. Phys. Lett. **103**, 232408 (2013).
[70] M. Koike, E. Shikoh, Y. Ando, T. Shinjo, S. Yamada, K. Hamaya, and M. Shiraishi, Appl. Phys. Express **6**, 023001 (2013).
[71] M. Ehlert, C. Song, M. Ciorga, M. Utz, D. Schuh, D. Bougeard, and D. Weiss, Phys. Rev. B **86**, 205204 (2012).
[72] A. Hoffmann, IEEE Trans. Magn. **49**, 5172 (2013).
[73] V. Vlaminck, J. E. Pearson, S. D. Bader, and A. Hoffmann, Phys. Rev. B **88**, 064414 (2013).
[74] V. Flovik, F. Macià, A. D. Kent, and E. Wahlström, J. Appl. Phys. **117**, 143902 (2015).
[75] J. W. P. Hsu, M. J. Manfra, R. J. Molnar, B. Heying, and J. S. Speck, Appl. Phys. Lett. **81**, 79 (2002).
[76] E. Shigematsu, Y. Ando, R. Ohshima, S. Dushenko, Y. Higuchi, T. Shinjo, H. J. von Bardeleben, and M. Shiraishi, Appl. Phys. Express **9**, 053002 (2016).
[77] P. Lubitz, J. J. Krebs, M. M. Miller, and S. Cheng, J. Appl. Phys. **83**, 6819 (1998).